

## Characterisation and Modelling of Particulate Composite with Flaky Aluminium Additives

Chethana P. Rao<sup>#</sup>, Harini Subramanian<sup>§</sup>, H. Murthy<sup>#</sup>, P.A. Ramakrishna<sup>#</sup> and Shantanu S. Mulay<sup>#,\*</sup>

<sup>#</sup>Indian Institute of Technology Madras, Chennai - 600 036, India

<sup>§</sup>Indian Institute of Technology Gandhinagar, Palaj - 382 355, India

\*E-mail: ssmulay@smail.iitm.ac.in

### ABSTRACT

The utilisation of flaky aluminium as an additive in the composite matrix has shown the ability to overcome the brittle nature encountered in epoxy resins. The additive increases the overall composite toughness without compromising its strength. The novelty of the present work is the demonstration of modelling the constitutive response of the particulate composite from the uniaxial tension tests conducted at three different displacement rates. Utilising two different mean-field homogenisation schemes (Dilute inclusion and Mori-Tanaka), the macro-scale properties were estimated and compared with the material constants obtained from experiments for this new particulate composite, which is proposed in the current study. The rate-independent response, at lower loading rates, is modelled by the elasto-plastic (EP) model, and the rate-dependent response, at higher loading rates, is modelled by elastic-viscoplastic (VP) model while capturing an inelastic deformation as seen in the fractographs. The EP and VP model material constants are then successfully obtained by optimisation employing the Levenberg–Marquardt algorithm and are eventually used in validating the experimental stress response.

**Keywords:** Aluminium; Particulate composites; Homogenisation; Composite matrix

### 1. INTRODUCTION

The high strength-to-weight ratio of epoxy-based composite materials makes them suitable for industries where overall weight reduction is crucial for fuel efficiency; some industries that are transitioning to composite materials are automotive, aerospace, packaging and electronics industries<sup>3-4,7</sup>. In the case of a composite with fibre reinforcements embedded in a polymer matrix, the fibre phase bears the load, and the matrix phase provides a continuum medium while holding the fibres together. The polymer matrix binds well with the reinforcements due to its good adhesive properties but is also brittle in nature. Epoxy is predominantly used as a matrix material for aerospace-grade composites. There is a need for novel lightweight materials to bear the primary loads and have good impact resistance. An increase in the ductility of epoxy, by the addition of flaky aluminium, ensures delayed damage rather than a sudden onset of failure, thereby improving the overall toughness of the resulting composite<sup>6</sup>.

The primary motivation of the current work is to achieve an overall reduction in brittleness while maintaining tensile strength, and this goal is achieved through the addition of flaky aluminium.<sup>6</sup> reported that adding a small weight fraction of flaky aluminium significantly improved the failure strain and tensile strength of the matrix by 200 % and 56 %, respectively. They also observed that the best enhancement of mechanical properties was obtained at 0.5 % wt fraction of flaky

aluminium. The present work thus uses this weight fraction for the constitutive modelling of uniaxial tensile response. The stiffness of the resulting particulate composite did not improve significantly, as the weight fraction of the flaky aluminium added was  $\approx 0.5$  %. Conventionally rigid additives increase the stiffness of matrix material at the cost of a decrease in the strain at failure, leading to increased brittleness within the homogenised material. On the contrary, as pointed out by<sup>6</sup>, when flaky aluminium is added to epoxy, it doubles the failure strain of the resulting particulate composite compared with the neat epoxy resin.

The primary objective of this work is to showcase the material characterisation of the proposed composite by first evaluating the material properties through mean-field homogenisation schemes (Dilute inclusion and Mori-Tanaka assumption, separately) and comparing their results with the corresponding values obtained from experiments.

Elasto-plastic (EP) and visco-plastic (VP) material models were developed to model the tension tests of the composite material at different loading rates. The Levenberg–Marquardt (LM) algorithm was employed to calibrate these material models based on the rate-dependent inelastic material response (currently lacking in literature). The clear demonstration of an iterative procedure to obtain EP and VP material constants employing nonlinear least square LM algorithm coupling with separate stress update MATLAB codes is the main novelty of this work.

It is observed from the uniaxial tension tests that the flaky aluminium composite material response is rate-independent

at lower loading rates (Fig. 1(a)), and it is rate-dependent at higher loading rates (Fig. 1(b)), having inelastic deformation at all times (as seen from fractographs). It is also clearly seen in Fig. 1 that the strain at failure is  $\approx 4.5\%$  as compared with the neat resin value of  $\approx 2\%$ ; the fractograph of the particulate composite also shows a rough surface, implying a ductile failure. This observation, based on the experimental stress-strain plots as well as fractographs, led to a choice of the EP model for the lower displacement rates and the VP model for the higher displacement rates during the constitutive material modelling.

The manuscript organisation is as follows. The experimental procedure and the corresponding results are given in Section 2, the material modelling details are given in Section 3, and the results are discussed in Section 4, followed by conclusions in Section 5.

## 2. EXPERIMENTAL PROCEDURE AND MATERIAL CHARACTERISATION

This section is focused on the experimental characterisation of flaky aluminium (FI-Al) additive composite in detail, with a primary focus on the response obtained under uniaxial tension for various loading conditions. The primary constituents of the particulate composite are aerospace-grade epoxy (Huntsman enterprise), tertiary amine (curing agent for epoxy), and flaky aluminium (additive) that enhances the ductility of neat epoxy resin. Studies from the literature have shown that significant enhancement in the properties of a neat resin with additives can only be achieved if their distribution in the resin is uniform and homogeneous (which is intuitive as well). This uniformity and homogeneity of the flaky aluminium additives in epoxy resin were ensured by overhead stirring and ultrasonication techniques. The post-curing cycle was also optimised, along with two different mixing techniques, for the increase in the effective material properties of the resulting flaky aluminium-epoxy composite. The FI-Al fillers are disc-shaped with an average particle size of around  $\approx 5\ \mu\text{m}$  and a thickness of around  $\approx 3\ \text{nm}$ , and they have a specific surface area of  $24\ \text{m}^2/\text{g}$ . The X-ray diffraction and Fourier-transform infrared spectroscopic studies showed that the flaky aluminium had little presence of

impurities or oxide, and their properties were similar to the bulk aluminium. The dimensions of flaky aluminium were obtained from the supplier's particle size analyser data, and the properties of flaky aluminium material were assumed to be the same as those of bulk aluminium material. The flaky aluminium shape and distribution were analysed by processing the scanning electron microscopy (SEM) images of FI-Al composite samples on ImageJ software. The SEM images were first converted to binary form (from greyscale) after enhancing the contrast between the inclusions and matrix phases. A detailed explanation regarding the fabrication and other techniques adopted can be found in Reference 6.

All the uniaxial tests are performed at 0.1-, 1-, and 10 mm/min displacement rates on the Zwick Roell (0.5 kN) universal testing machine till the final specimen failure. The strain field was measured using the Digital Image Correlation technique (DIC). The images for strain field measurements were captured using two Prosilica GX191 cameras. The strain field was obtained using Vic2d software for postprocessing the images. The specimen dimensions and the tensile test procedure are followed according to ASTM D 638 standard.

Five samples (prepared in the same batch) were used for each displacement loading rate to obtain the standard deviation in the results. Figure 1(a) shows the experimental results for the 1 mm/min displacement loading rate for different samples. Figure 1(b) shows the experimental stress-strain plots at various loading rates (showing a typical curve for each loading rate). It is important to observe from Fig. 1 that (1) there is repeatability in the results for the same loading rate, (2) the results are dependent on the displacement rate of loading above a certain loading rate, and (3) an inelastic deformation (ridge patterns) is seen in all the fractographs (even at lower loading rates) obtained from the failed specimen. It is seen from Fig. 1(b) that the material response is overlapping up to the proportional limit (20-30 MPa) for all the loading rates, eventually resulting in plastic deformation (visco-plastic behaviour, as seen in fractograph and Fig. 2(b)).

These experimental observations prompted the assessment of the suitability of a rate-independent material model at lower displacement rates of loading and a rate-dependent model

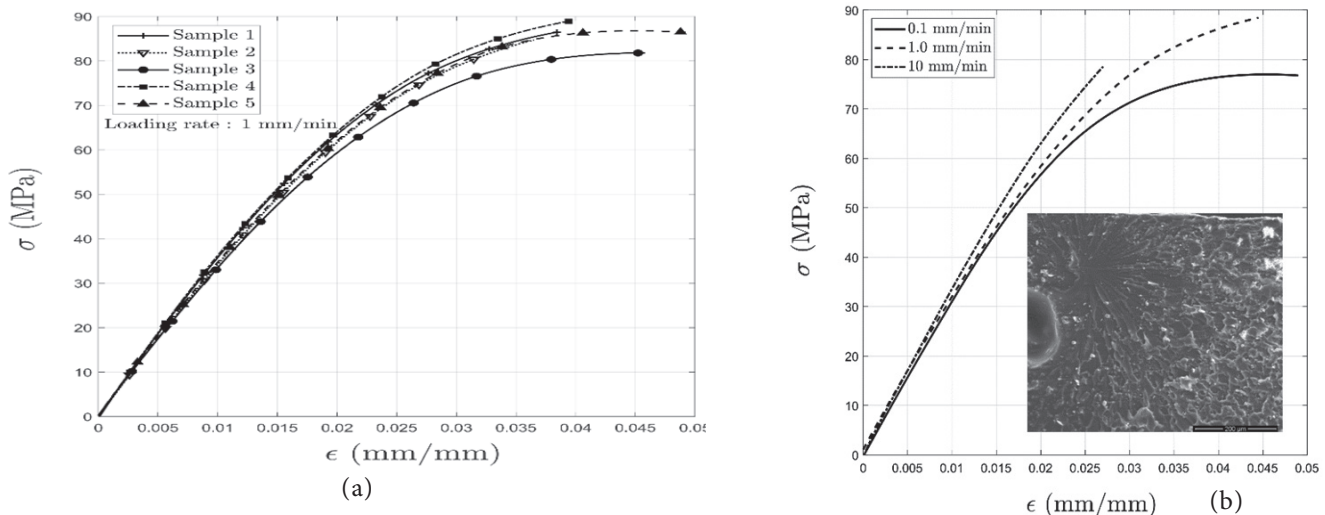


Figure 1. Experimental uniaxial response of flaky aluminium-epoxy composite: (a) loading at 1 mm/min. displacement rate, and (b) loading at different displacement rates.

at higher displacement rates of loading while modelling the FI-Al particulate composite in the next section. The uniaxial tensile tests, conducted at different displacement loading rates, revealed a change in the ultimate stress and strain at failure (Fig. 1(b)). With the increase in loading rate, a slight increase in the ultimate stress and a decrease in the failure strain were observed with an increase in the loading rate. This is a characteristic behaviour of rate-dependent material. An increase in the displacement loading rate provides less time to trigger a viscous response, and the response is primarily elastic in nature. A lower displacement loading rate allows the material to exhibit a viscous (time-dependent) response, leading to visco-elastic or visco-plastic behaviour. The present FI-Al particulate composite has epoxy resin (showing viscous /quasi-brittle behaviour depending on loading rate) and flaky aluminium additives (showing elastic-ductile behaviour). The constitutive behaviour of the resulting FI-Al particulate composite is visco-elastic/visco-plastic in nature, thus resulting in the rate-dependent experimental response.

**3. MATERIAL MODELLING**

The experimental results of the FI-Al composite were discussed previously, and their constitutive modelling is explained in this section. Figure 1 shows that the FI-Al composite exhibits viscoplastic behaviour at higher loading rates and the response is independent of the loading rate at lower displacement rates of loading. The inelastic material response is seen from the failure surfaces of the specimen (as seen in fractography). A comparison of the uniaxial response of the particulate composite and the neat epoxy specimen is shown in Fig. 2. It can be observed from Fig. 2 that the longitudinal and transverse strains (obtained by DIC),  $\epsilon_{xx}$  and  $\epsilon_{yy}$ , respectively, are multiplied with an initial slope of the stress-strain curve and plotted along with the original stress  $\sigma_{xx}$  for both the neat epoxy (Fig. 2(a)) and FI-Al composite (Fig. 2(b)) specimens. It is important to observe in Fig. 2(a) that (1) the scaled transverse strain  $\epsilon_{yy}$  in neat epoxy specimen increases fairly linearly along with the scaled longitudinal

strain  $\epsilon_{xx}$ , implying a linearly elastic behaviour until complete failure of the specimen, and (2) scaled  $\epsilon_{xx}$  is overlapping with actual  $\sigma_{xx}$  almost until complete failure implying no trace of inelastic strain/deformation in the case of neat epoxy specimen (also seen in fractographs having a clean and shining fracture surface perpendicular to loading direction).

It is important to observe in Fig. 2(b) that (1) the scaled longitudinal strain  $\epsilon_{xx}$  quickly deviates from actual  $\sigma_{xx}$  (probably from the proportional limit point around 25 MPa), and (2) both scaled  $\epsilon_{xx}$  and  $\epsilon_{yy}$  start having nonlinear growth/progression until breakpoint of the material, which one can deduce from this observation that there is presence of inelastic strain after yield point of the particulate composite. The inelastic deformation is quite apparent with the increase in the displacement loading rate.

The evidence of inelastic strain/deformation, in the case of the FI-Al composite specimen, becomes significant at higher displacement rates of loading. The above-explained experimental evidence is utilised while planning the material modelling of the FI-Al composite in three steps: (1) Estimation of macro-scale properties of the composite from material homogenisation schemes (Section 3.1), (2) elasto-plastic modelling with an exponential hardening law (at lower loading rates) (Section 3.2), and (3) viscoplastic modelling utilising Peric’s law (at higher loading rates) (Section 3.3) is explained in the following subsections. The main novelty of this work is that it demonstrates a procedure to obtain EP and VP material constants employing nonlinear least square LM algorithm coupling with a separate stress update MATLAB code (as explained in Fig. 3(a)).

**3.1 MATERIAL HOMOGENISATION**

The FI-Al composite is treated as a matrix with spherical inclusions for a preliminary study (individual phases are isotropic). The micro-scale properties of flaky aluminium are considered  $E_{flake} = 68$  GPa and  $\nu_{flake} = 0.32$ , and epoxy matrix properties are  $E_m = 3.4$  GPa and  $\nu_m = 0.37$ . The mean field homogenisation concentration and Eshelby tensors are

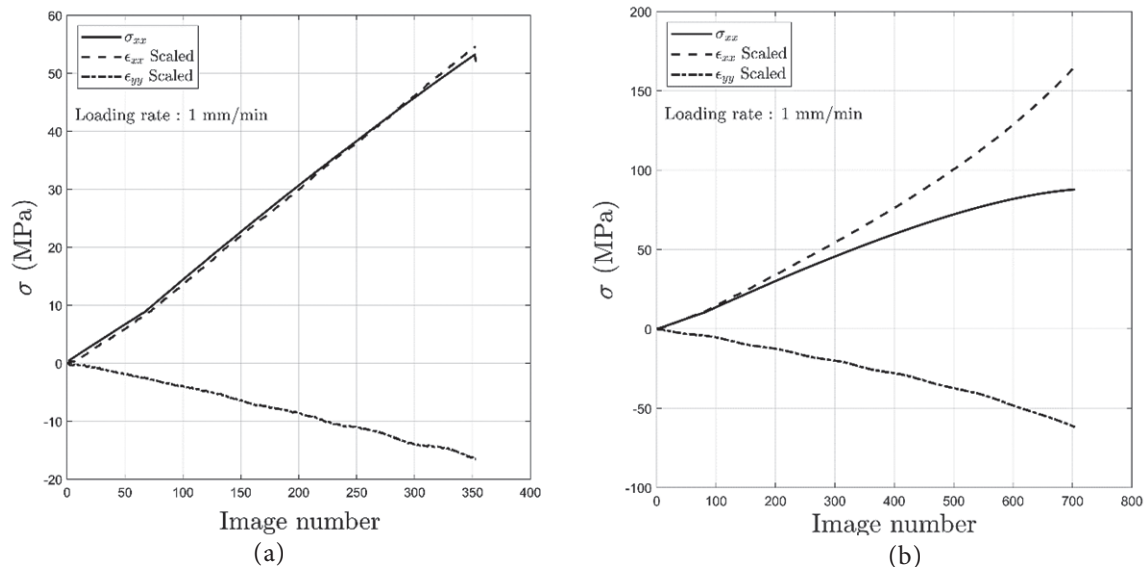
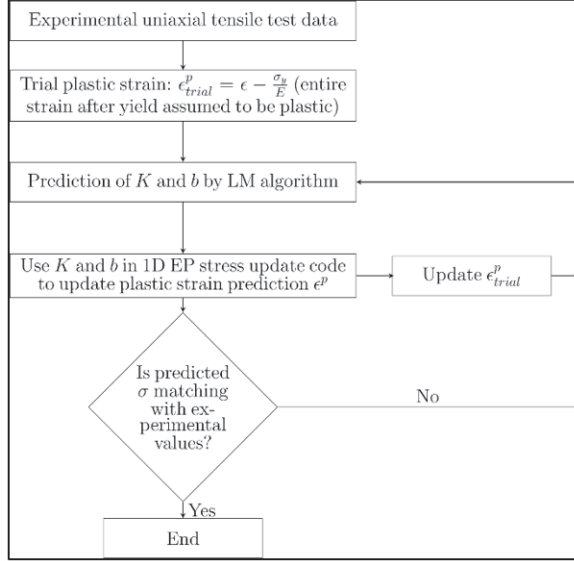


**Figure 2. Comparison of actual  $\sigma_{xx}$  with scaled values of longitudinal ( $\epsilon_{xx}$ ) and transverse ( $\epsilon_{yy}$ ) strains for (a) pure epoxy sample, and (b) 0.5 % flaky aluminium-epoxy composite.**

**Table 1. Macro-scale Fl-Al properties (0.5 % wt aluminium flakes)**

Material parameters	Experimental values	Mori-Tanaka	Dilute-inclusions
$E_{11}$	$3.89^{\pm 0.18}$	3.4147	3.4078
$\nu_{12}$	$0.36^{\pm 0.01}$	0.3698	0.3698
$\nu_{13}$	$0.39^{\pm 0.08}$	0.3698	0.3698

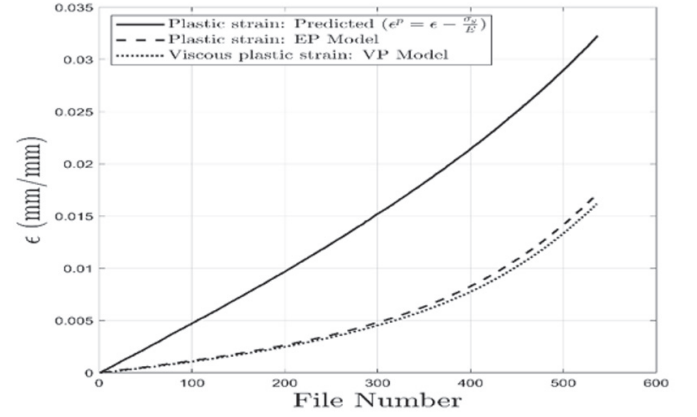


(a)

both models, the macro-scale properties from Table 1 were incorporated.

### 3.2 Rate-Independent Constitutive Modelling

A one-dimensional (1D) rate-independent model (elasto-plastic model with exponential isotropic hardening, is implemented to characterise the uniaxial loading response of



(b)

Figure 3. (a) Flowchart explaining a procedure to obtain EP model constants from experiments coupling LM algorithm with stress update code, (b) inelastic strain  $\epsilon^p$  comparison obtained by EP and VP models (Table 2).

#### 1. Elastic predictor : Given the strain increment $\Delta\epsilon$

$$(\epsilon^e)_{n+1}^{tr} = (\epsilon^e)_n^{tr} + \Delta\epsilon_{n+1}, \sigma_{n+1}^{tr} = E(\epsilon^e)_{n+1}^{tr}, f_{n+1}^{tr} = \sigma_{n+1}^{tr} - (\sigma_y)_{n+1}^{tr},$$

where  $(\sigma_y)_{n+1}^{tr} = \sigma_{y0} + K[1 - \exp(-br_{n+1}^{tr})]$

#### 2. Yield criterion

if  $f_{n+1}^{tr} \leq 0$ ,  $(\bullet)_{n+1} = (\bullet)_{n+1}^{tr}$ ,  $\Delta\gamma = 0$  and exit stress update else go to Step 3.

#### 3. Plastic corrector

Compute  $\Delta\gamma$ :  $f_{n+1}^{tr} + (\sigma_y)_{n+1}^{tr} - \sigma_y(r_n + \Delta\gamma) - E\Delta\gamma = 0$  (by Newton-Raphson method)

#### 4. Update

$$\Delta\epsilon_{n+1}^p = \Delta\gamma \text{sign}(\sigma_{n+1}^{tr}), \Delta\epsilon_{n+1}^e = \Delta\epsilon_{n+1} - \Delta\epsilon_{n+1}^p, r_{n+1} = r_n + \Delta\gamma, \sigma_{n+1} = E(\epsilon_{n+1} - \epsilon_{n+1}^p)$$

Check:  $f_{n+1} = \sigma_{n+1} - (\sigma_y)_{n+1} = 0$

#### 5. Exit

Box 3.1: Stress update return mapping algorithm for elastic-plastic model.

obtained for a spherical inclusion (0.5 % weight fraction of aluminium flakes), and macro-scale material property estimates are given in Table 1<sup>1,5,8</sup>. The  $E_{11}$ , obtained by homogenisation, is slightly higher than the experimental value primarily due to the approximated spherical inclusion shape.

It can be deduced from these results that the particulate composite exhibits rate-dependent characteristics, such as inelastic strain at a higher displacement loading rate. Based on this observation, the material is initially modelled using a rate-independent model, such as the Elasto-Plastic model at lower displacement loading rates, and this method is further extended into modelling with a rate-dependent model (viscoplastic); for

the Fl-Al composite. The one-dimensional total strain and the constitutive relation can be represented as:

$$\sigma = E(\epsilon - \epsilon^p), \epsilon = \epsilon^e + \epsilon^p \quad (1)$$

where,  $\epsilon$  is the total strain, and  $\epsilon^e$ ,  $\epsilon^p$  are the elastic-, plastic parts, respectively.  $E$  is the Young's modulus. The yield criterion ( $f$ ) for the EP model is

$$f = |\sigma| - \sigma_y, \text{ where } \sigma_y = \sigma_{y0} + K(1 - \exp(-br)) \quad (2)$$

where,  $\sigma_{y0}$  is an initial yield stress,  $b$  and  $K$  are the material constants in the exponential isotropic hardening law, and  $r$  is the accumulated equivalent plastic strain. The normality law

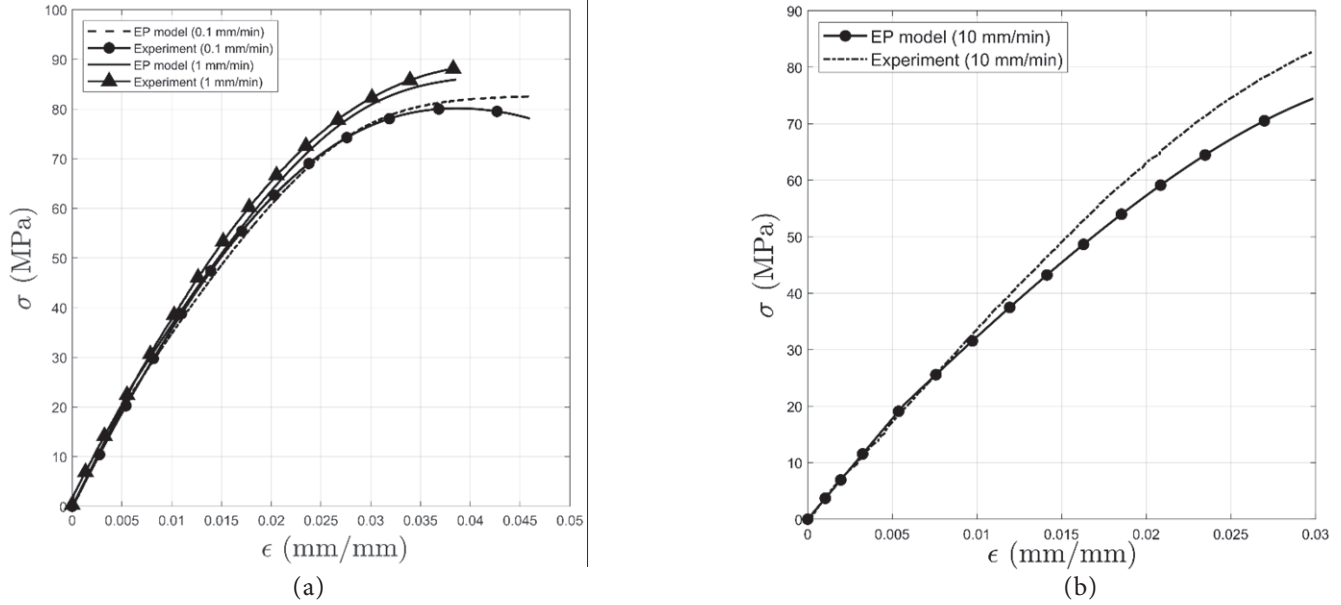


Figure 4. Comparison of EP model  $\sigma$  vs  $\epsilon$  prediction with experimental response: (a) 0.1 and 1 mm/min, and (b) 10 mm/min displacement rates.

1. **Elastic predictor : Given the strain increment  $\Delta\epsilon$**   
 $(\epsilon^e)_{n+1}^{tr} = (\epsilon^e)_n^{tr} + \Delta\epsilon_{n+1}$ ,  $\sigma_{n+1}^{tr} = E(\epsilon^e)_{n+1}^{tr}$ ,  
 $f_{n+1}^{tr} = \sigma_{n+1}^{tr} - (\sigma_y)_{n+1}^{tr}$ , where  $(\sigma_y)_{n+1}^{tr} = \sigma_{y0} + K[1 - \exp(-br_{n+1}^{tr})]$
2. **Yielding criterion**  
 if  $f_{n+1}^{tr} \leq 0$ ,  $(\bullet)_{n+1} = (\bullet)_{n+1}^{tr}$ ,  $\Delta\gamma = 0$  and exit stress update  
 else go to Step 3.
3. **Viscoplastic corrector**  
 Compute  $\Delta\gamma$ : Solve  $\Delta\gamma - \frac{\Delta\epsilon}{\mu} \left[ \left( \frac{(\sigma_{n+1}^{tr} - E\Delta\gamma)}{\sigma_y(r_n + \Delta\gamma)} \right)^{\frac{1}{\zeta}} - 1 \right] = 0$  (by Newton-Raphson method)
4. **Update**  
 $\Delta\epsilon_{n+1}^{vp} = \Delta\gamma \text{sign}(\sigma_{n+1}^{tr})$ ,  $\Delta\epsilon_{n+1}^e = \Delta\epsilon_{n+1} - \Delta\epsilon_{n+1}^{vp}$ ,  $r_{n+1} = r_n + \Delta\gamma$ ,  $\sigma_{n+1} = E(\epsilon_{n+1} - \epsilon_{n+1}^{vp})$
5. **Exit**

Box 3.2: Stress update return mapping algorithm for a visco-plastic model.

as  $\epsilon^p = \gamma \text{sign}(\sigma)$  is used for the plastic strain evolution. The stress update algorithm for the EP model from the predictor/corrector scheme, shown in Box 3.1, is used in tandem with the LM algorithm, explained in Fig. 3(a), while computing  $K$  and  $b$  hardening constants [Eqn. (2)]. The coupled algorithm, as given in Fig. 3(a), is explained as follows. A trial plastic strain is computed from experimental data, and the plasticity parameters are computed by the LM algorithm (by stress fitting). The plastic strain prediction is improved by inputting these parameters into the 1D stress update code. The LM and stress update codes are thus used iteratively till the uniaxial stress-strain response closely matches (within an acceptable tolerance) the experimental plot. A similar procedure is adopted while obtaining VP model parameters from the experimental data.

### 3.3 Rate-Dependent Material Response Modelling

Figure 1 shows the presence of inelastic strain in both the mechanical response and the fractography, this is more

prevalent at higher rates of loading, and based on these phenomena, the Peric's model for viscoplastic response<sup>2</sup> is used in this study. The hardening law used in the EP model continues to be used for this particular model, albeit the flow rule used is different and is defined as:

$$\begin{aligned} \epsilon^{vp} &= \dot{\gamma} \text{sign}(\sigma), \text{ where } \dot{\gamma}(\sigma, \sigma_y) = \\ &= \frac{1}{\mu} \left[ \left( \frac{|\sigma|}{\sigma(\epsilon^{vp})} \right)^{\frac{1}{\zeta}} - 1 \right], \text{ if } f_{n+1}^{tr} \geq 0 \wedge \\ &= 0, \text{ if } f_{n+1}^{tr} < 0 \end{aligned} \quad (3)$$

The 1D constitutive relation is the same as mentioned in Eqn. (1) and for the case of the VP model replacing  $\epsilon^p$  by  $\epsilon^{vp}$ . The yield criterion is the same as Eqn. 2, with  $f > 0$  that estimates the excess stress, and the VP material constants are  $\mu$  and  $\zeta$  (greater than 0).

The algorithm for the rate-dependent model is described in Box 3.2. The time interval  $[t_n, t_{n+1}]$  is considered with  $\Delta t = t_{n+1} - t_n$ .

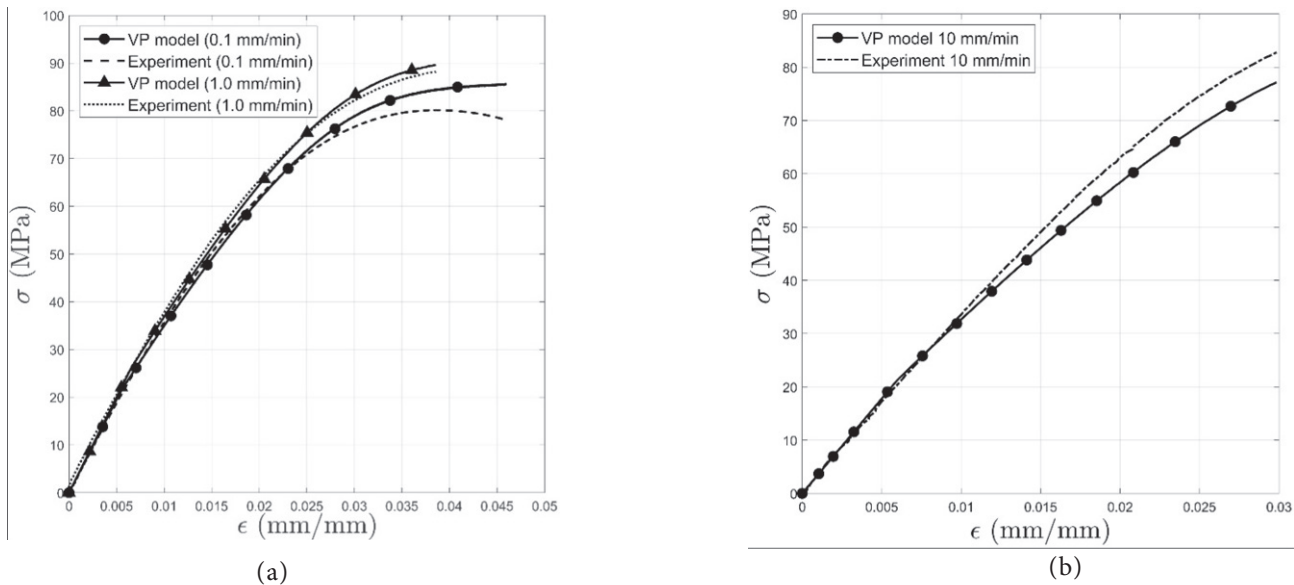


**Figure 5. Validation of VP model  $\sigma$  vs  $\epsilon$  estimation against experiment results: (a) 0.1 and 1 mm/min, and (b) 10 mm/min, displacement rates.**

#### 4. RESULTS AND DISCUSSION

The response of the particulate composite under uniaxial tensile load at different displacement loading rates is shown in Fig. 1(b), clearly implying a loading rate dependency (inelastic deformation in fractographs). The authors postulated rate-independent and dependent behaviours at lower and higher displacement rates, respectively, as explained at the beginning of Section 3. All material constants are obtained by the LM method, as explained in Fig. 3(a), minimising stress-based residual functions (Boxes 3.1 and 3.2) employing experimental strain and time histories. The trial  $\epsilon^p$  in the EP model is obtained by  $\epsilon^p = \epsilon - (\sigma_{y0}/E)$ , which is used in the LM method to obtain EP constants  $K$  and  $b$ . These constants are used in the EP model stress-update code (Box 3.1) to compute the stress. If the model stress varies more than 5 % from the experiment, EP model  $\epsilon^p$  is used in the LM method for a better prediction of  $K$  and  $b$ . This iterative process is performed for five 1 mm/min displacement rate samples, and the average values of  $K$  and  $b$  parameters are obtained (Table 2).

**Table 2. Material constants computed from experiments (mean values)**

Elastic modulus $E$ (GPa)	Yield stress $\sigma_{y0}$ (MPa)	EP model parameters			VP model parameters	
		$K$ (MPa)	$b$	$\mu$	$\zeta$	
3.89	26.2	61.8	234	$2.71 \times 10^6$	$6.05 \times 10^{-3}$	

Figure 3(b) shows a significant difference in the trial  $\epsilon^p$  from the experiment, and the converged  $\epsilon^p$  and  $\epsilon^{vp}$  were obtained by EP and VP models, respectively (by average values of  $K$  and  $b$ ), thus justifying the iterative process proposed in the present work, while updating the inelastic strain. The trial  $\epsilon^{vp}$  for the VP model is thus taken as converged  $\epsilon^p$  by the EP model while computing VP constants. This ensures the values of  $(\sigma \nu \sigma_y(\epsilon^{vp})) > 1$  (necessary condition) at all time increments, thus

satisfying Eqn. (3). The VP constants,  $m$  and  $\zeta$ , are obtained by three specimens response and their mean value is given in Table 2. Both models, EP and VP, performed well in capturing the uniaxial response of 0.1 mm/min and 1 mm/min displacement rates, as shown in Fig. 4 and 5. VP model, however, did well for a 10 mm/min displacement rate (Fig. 5(b)), thus justifying an initial postulate that the rate-dependent behaviour of novel Fl-Al composite is more prominent at higher displacement loading rates. It is thus seen that the proposed novel material has VP behaviour at higher loading rates. Despite the VP model performing better than the EP model for a 10 mm/min loading rate, there is a slight difference between the numerical and experimental results. The authors postulate that the possible reason for this difference is two key aspects of mechanics playing a role: (1) rate-dependent constitutive response and (2) finite deformation of the material. The experimental characterisation clearly shows the rate-dependent response of the Fl-Al particulate composite (Fig. 1(b)). The finite deformation aspect begins to play a role as soon as the necking (gauge section area decreasing) begins (irrespective of an applied displacement loading rate, even at 0.1 mm/min.). The necking usually starts very late when the specimen is loaded at low displacement rates, i.e., 0.1 and 1 mm/min., while it starts early at a higher displacement rate, i.e., 10 mm/min. The Fl-Al particulate composite, however, undergoes significant necking at a 10 mm/min displacement loading rate, thus warranting a constitutive model accounting for the large deformation. This need could be why the presented models cannot fully capture the experimental response at a 10 mm/min loading rate (even though the rate dependency is accounted for).

#### 5. CONCLUSIONS

It was observed that the addition of flaky aluminium improved the overall material properties by reducing the brittle nature and increasing the tensile strength of the Fl-Al composite. The response of the Fl-Al particulate

composite under the uniaxial tensile test is obtained at varied displacement rates, and possible failure causes and evidence of inelastic strain at the micro-scale are identified by studying the fractographs. The macro-scale composite properties are obtained by Mori-Tanaka and dilute estimates, and they are validated against experiments. The constitutive response of the novel FI-Al composite is further established by elasto-plastic and viscoplastic models; thus, variation in material response with a change in displacement rate is captured.

## REFERENCES

1. Böhm, Helmut J. A short introduction to basic aspects of continuum micromechanics. Cdl-fmd Report 3, 1998.
2. Neto, De Souza; Eduardo, A.; Peric, Djordje & David, R.J. Owen. Computational methods for plasticity: Theory and applications. John Wiley & Sons, 2011.
3. Gibson, Ronald F. Principles of composite material mechanics. CRC Press, 2016.
4. Mallick, Pankar K. Fiber-reinforced composites: materials, manufacturing, and design. CRC Press, 2007.
5. Qu, Jianmin & Cherkaoui, Mohammed. Fundamentals of micromechanics of solids, 2006, **735**, Wiley, Hoboken.
6. Rao, Chethana P.; Periyapatna, Ramakrishna & Murthy, Haradanahalli. Effect of high aspect ratio flaky aluminum on mechanical properties of epoxy-based particulate composites. *J. Vinyl and Additive Technol.*, 2021, **27**(4), 711-721.
7. Soutis, C. Fibre reinforced composites in aircraft construction. *Progress in Aerospace Sci.*, 2005, **41**(2), 143-151.
8. Udhayaraman, R. & Shantanu S. Mulay. Multi-scale damage framework for textile composites: Application to plain woven composite. *Eu. J. Mechanics-A/Solids*, 2019, **77**, 103809.

## CONTRIBUTORS

**Dr Chethana P. Rao** is an Aerospace Engineer and obtained her PhD in aerospace engineering from the IIT Madras, Chennai, India. Her primary work was on material modelling and material failure prediction using diffused crack-based models. Her present work in University of Galway, Ireland, involves developing deep learning models to predict brain tissue deformation under impact load.

His contributions include conceptualization (experiments), validation, investigation, procurement of resources (experiments),

supervision, and funding acquisition in the current study.

**Dr Harini Subramanian** is an Assistant Professor in the Department of Mechanical Engineering at IIT Gandhinagar. She obtained her PhD in aerospace engineering from IIT Madras, Chennai, India. Her research interests include: constitutive modelling of materials, continuum damage mechanics, mechanics of composites, and self-healing materials. Her present work is focused on progressive damage analysis of fibre-reinforced composites and the development of phase field method-based crack propagation models for inelastic materials.

Her contributions include in methodology development, software implementation, validation, formal analysis, data curation, visualization and, writing the original draft in the current study.

**Prof H. Murthy** is a Professor in the Department of Aerospace Engineering at IIT Madras. He obtained his PhD at Purdue University. He has been a faculty at IIT Madras since 2004. His main fields of interest are contact mechanics and tribology, fretting fatigue, damage mechanisms in metals & composites and material modelling. Further, he is interested in optimisation of design to reduce weight in Aerospace structures.

His contributions include conceptualization (experiments), validation, investigation, procurement of resources (experiments), supervision, and funding acquisition in the current study.

**Dr P.A. Ramakrishna** obtained his PhD from Indian Institute of Science, Bengaluru. He is currently working as a Professor in Aerospace Engineering department at IIT Madras. His areas of interest include: solid propellant combustion and develop systems with extending range of ramjets with use of highly dense fuel rich solid propellants.

His contributions include conceptualization (experiments), validation, investigation, procurement of resources (experiments), supervision, and funding acquisition in the current study.

**Dr Shantanu S. Mulay** is a Professor in the Department of Aerospace Engineering at IIT Madras. He obtained his PhD in school of Mechanical and Aerospace Engineering from Nanyang Technological University, Singapore. He joined Aerospace Engineering department of IIT Madras, as an Assistant Professor. His research interests include: Material modelling (composites, viscoelastic, granular, and soft materials), continuum damage-healing mechanics, fracture mechanics, and development of numerical meshless methods.

His contributions include conceptualization (modelling), methodology development (modelling), software implementation, validation, investigation, procurement of resources (computational tools), writing the original draft, and supervision (modelling and manuscript flow) in the current study.